

# 1Potential of ligand-promoted dissolution at mild pH for 2the selective recovery of rare earth elements in bauxite 3residue

4Claire Lallemand<sup>†</sup>, Jean Paul Ambrosi<sup>†</sup>, Daniel Borschneck<sup>†,O</sup>, Bernard Angeletti<sup>†,O</sup>, Perrine  
5Chaurand<sup>†,O</sup>, Andrea Campos<sup>‡</sup>, Morgane Desmau<sup>§</sup>, Till Fehlaue<sup>†</sup>, Mélanie Auffan<sup>†,^</sup> Jérôme  
6Labilie<sup>†</sup>, Nicolas Roche<sup>†,∇</sup>, Laurent Poizat<sup>||</sup>, Blanche Collin<sup>†,O</sup>, Jérôme Rose<sup>†,^</sup>, Clément  
7Levard<sup>†,O</sup>

8<sup>†</sup>Aix Marseille Univ, CNRS, IRD, INRAE, CEREGE, Aix-en-Provence 13545, France

9<sup>‡</sup>Aix Marseille Univ, CNRS, Centrale Marseille, FSCM (FR1739), CP2M, 13397 Marseille,  
10France

11<sup>§</sup> Deutsches Elektronen-Synchrotron DESY 22607, Hamburg, Germany

12<sup>^</sup>Duke university, Civil and Environmental Engineering department, Durham, USA

13<sup>||</sup>Alteo Environnement, Gardanne, France

14<sup>∇</sup>INternational Water Research Institute (IWRI), Mohammed VI Polytechnic University, Ben  
15Guerir 43150, Morocco

16<sup>O</sup>Laboratoire Mixte International Activité Minière Responsable “LMI-AMIR”,  
17IRD/UM5/INAU, 10000 Rabat, Morocco

18Jean Paul Ambrosi : [ambrosi@cerege.fr](mailto:ambrosi@cerege.fr)

19Daniel Borschneck : [borschneck@cerege.fr](mailto:borschneck@cerege.fr)

20Bernard Angeletti : [angeletti@cerege.fr](mailto:angeletti@cerege.fr)

21Perrine Chaurand : [chaurand@cerege.fr](mailto:chaurand@cerege.fr)

22Andrea Campos : [andrea.campos@univ-amu.fr](mailto:andrea.campos@univ-amu.fr)

23Morgane Desmau : [morgane.desmau@gmail.com](mailto:morgane.desmau@gmail.com)

24Till Fehlaue : [fehlaue@cerege.fr](mailto:fehlaue@cerege.fr)

25Mélanie Auffan : [auffan@cerege.fr](mailto:auffan@cerege.fr)

26Jérôme Labille : [labille@cerege.fr](mailto:labille@cerege.fr)

27Nicolas Roche : [roche@cerege.fr](mailto:roche@cerege.fr)

28Laurent Poizat : [Laurent.POIZAT@alteo-alumina.com](mailto:Laurent.POIZAT@alteo-alumina.com)

29Blanche Collin : [collin@cerege.fr](mailto:collin@cerege.fr)

30Jérôme Rose : [rose@cerege.fr](mailto:rose@cerege.fr)

31Clément Levard : [levard@cerege.fr](mailto:levard@cerege.fr)

32

33**Key words:** Bauxite Residue (BR); Circular Economy; Rare Earth Elements (REEs); Low  
34Molecular Weight Organic Acids (LMWOAs); Ligand-promoted Dissolution;  
35Characterization, Critical Elements, Speciation.

36

## 37Abstract

38In a context of overexploitation of natural resources, a circular economy and particularly the  
39extraction of resources from secondary sources, are essential to sustain a number of key  
40technologies including renewable energies. Among secondary sources, bauxite residue  
41contains critical elements including rare earth elements (REEs) (712mg/kg). We investigated  
42the use of soft and selective dissolution protocols at mild pHs (2-6) as an alternative to pyro-  
43and hydrometallurgy for the recovery of REEs through ligand-promoted dissolution. This  
44approach depends on the detailed characterization of the waste and the speciation of targeted  
45elements. We assessed dissolution using low molecular weight organic acids (LMWOAs) and  
46their conjugate bases. Citric acid/citrate showed satisfactory dissolution of REEs (up to 50%  
47of light REEs) up to a pH of nearly 5, while tartaric acid/tartrate showed the best dissolution  
48selectivity (enrichment factor up to 21.5 compared to Fe, Al and Ti). Almost no heavy REEs  
49were dissolved in any of the conditions tested, probably due to the high chemical stability of  
50their bearing phases. Indeed, heavy REEs were found as discrete phosphate particles.

51

## 52Synopsis

53Ligand-promoted dissolution, an interesting mechanism for the development of selective  
54recovery processes of REEs from bauxite residue in mild pH conditions.

55

## 56Introduction

57The world population has increased fivefold since the 1900s, leading to overexploitation of  
58the Earth's primary resources. Metals are one of these resources, particularly the critical  
59metals used in modern technologies (smartphones, electronic compounds, wind turbines,  
60permanent magnet, electric cars, etc.) because of their unique physical and chemical  
61properties<sup>1</sup>. These critical elements combine high economic value (in terms of end-use  
62applications) and high risk of disruption in supplies due to limited reserves and geopolitical  
63considerations<sup>2,3</sup>.

64Among these metals, rare earth elements (REEs), including lanthanides, yttrium (Y) and  
65scandium (Sc), are among the most critical in Europe. Global consumption increased from 80  
66000 tons of rare earth oxides in 2000 to 140 000 tons in 2019<sup>1</sup>. REEs are often separated into  
67two subgroups according to their different physico-chemical properties: La, Ce, Pr, Nd, Sm,  
68Eu and Gd are classified as light rare earth elements (LREEs) and Tb, Dy, Ho, Er, Tm, Yb,  
69and Lu are classified as heavy rare earth elements (HREEs). Yttrium and Sc are often  
70included in the REE group because of their similar physico-chemical properties. Although Sc  
71often behaves differently than other REEs, partly due to its smaller radius (for example, it can  
72replace iron in goethite<sup>4</sup>). Yttrium behavior is very similar to that of HREEs (similar ionic  
73radii and valence state).

74Most REEs are produced in China, which accounts for 86% of world production (average  
752012-2016, EU report 2020), and is also the world's largest consumer and exporter<sup>5</sup>. REEs  
76are almost entirely produced by extraction from natural ores, mostly using controversial  
77methods with negative sanitary (radioactivity, corrosivity) and environmental impacts  
78(water/soil contamination)<sup>6</sup>. This mining industry is also a particularly big consumer of  
79energy, water, and chemicals, and produces effluents and solid wastes that are intentionally or  
80accidentally released into the environment<sup>6</sup>. In this context, there is an urgent need to find  
81alternatives for the production of REEs to reduce (i) the supply risk and (ii) the environmental  
82and sanitary impacts associated with their extraction.

83In circular economy, mining and industrial wastes represent secondary REE resources that are  
84largely under-exploited partly because of the low cost of extracting REEs from natural ores  
85and the lesser quality of secondary sources compared to natural ones. However, given the  
86strong pressure on these metals, mining secondary sources may become a sustainable source  
87of REEs in the near future. Among secondary sources, bauxite residues (BR), also known as  
88red mud when hydrated, are an attractive source of REEs. BR is an industrial waste resulting

89from the extraction of alumina from natural bauxite rocks using the Bayer process (soda  
90leaching). For example, a Jamaican residue contains up to 2,500 mg/kg of REEs <sup>7</sup> which is  
91about 10 times higher than the natural abundance of REEs in the Earth's crust <sup>8</sup>. Extracting  
92REEs from BR is a real economic and environmental challenge. Existing processes, usually  
93based on the leaching of REEs from BR, use strong mineral acids such as hydrochloric, nitric,  
94or sulfuric acids <sup>9,10</sup>. During acidification, proton-promoted dissolution digests most of the  
95matrix with poor REE selectivity, requires post-leaching purification steps, and produces large  
96quantities of hazardous acidic liquid and solid wastes.

97The use of low molecular weight organic acids (LMWOAs) as alternatives to the strong acids  
98traditionally used in hydro- or pyro-metallurgy, has been less studied, partly due to their lower  
99leaching efficiency. Leaching efficiency reported in the literature using LMWOAs rarely  
100exceeds 50% for LREEs and 65% for HREEs <sup>11,12</sup> (*see S1 in SI*) whereas strong acids usually  
101dissolve 80-90% of REEs <sup>13</sup>. However, although less efficient, leaching with LMWOAs  
102involving ligand-promoted dissolution has other advantages that deserve more attention with a  
103view to designing more sustainable extraction strategies. In particular, ligand-promoted  
104dissolution is expected to be more selective (i.e., to require fewer extraction steps and to  
105produce less waste) and can be performed at more neutral pH (hence producing non-acidic  
106solid and liquid wastes). However, developing such processes requires a better understanding  
107of the speciation of the REEs, the identification of the bearing phases in the matrix, which we  
108investigate here. In particular, ligand-promoted dissolution depends to a great extent on the  
109specific affinity of LMWOAs for the surface of minerals and for the element in solution,  
110which will be strongly affected by pH.

111The aim of our study was to investigate the potential of ligand-promoted dissolution for the  
112selective leaching of REEs in BR in mild conditions. We performed multi-scale  
113characterization of the BR including the speciation of REEs (chemical composition,  
114mineralogy, particle size, elemental distribution, speciation), and assessed the effects of a  
115number of experimental variables including the nature of the LMWOAs and pH on  
116dissolution efficiency and selectivity. For the first time, speciation of HREEs in bauxite  
117residue has been described at the bulk scale and pH-dependent dissolution behavior has been  
118reported. In light of these results, ligand-promoted dissolution mechanisms are discussed with  
119a view to improving dissolution selectivity and yield in future work.

120

121

122

## 123Material and methods

### 124Material

125The BR we studied came from Bouc-Bel-Air (South of France). It was produced and collected  
126in February 2019 and stored in sealed plastic containers at ambient temperature until required.  
127The fresh BR was sampled immediately after the chemical extraction of alumina (Bayer  
128process) from bauxite, a lateritic deposit, originating from Guinea (West Africa). Before the  
129experiments, the BR was dried at 60-70 °C for 2 days, manually ground in an agate mortar,  
130sieved to 125µm and homogenized using an orbital shaker before use. The effect of different  
131BR grinding methods on dissolution efficiency was further studied and is presented in SI (*see*  
132*S2 in SI*)

133

### 134Characterization of the bauxite residue

135**Chemical composition.** Four samples of the same dry and ground BR were mineralized using  
136the alkaline fusion method: 100 mg of BR and 500 mg of dry lithium tetraborate (flux) were  
137mixed and heated at 1 000 °C in an oven. The resulting fusion bead was dissolved in 40ml of  
138nitric acid (1N). The final solutions were diluted in 2% nitric acid at a dilution factor of 200  
139and trace elements and minor elements including REEs were analyzed with a Perkin Helmer  
140300X quadrupole ICP-MS for, while major elements were analyzed with a Perkin Elmer ICP-  
141OES Optima 4300 DV. The results (concentration in mg/kg) are expressed along with the  
142average and the standard deviation of the 4 samples.

143**Mineralogy of the bauxite residue.** X-Ray diffraction was performed at 40 kV and 40mA on  
144a Panalytical X'Pert Pro  $\theta$ - $\theta$  diffractometer equipped with a rear monochromator and a cobalt  
145anticathode ( $K_{\alpha} = 1.79\text{\AA}$ ). Scans were made between 5° and 75° (2 $\theta$ ) with a step size of  
1460.033°. The sample was rotated at 15 rpm during analysis to improve the statistics.

147**Spatial distribution of REEs.** Scanning electron microscopy coupled with EDX analysis  
148(SEM-EDX) and Nano X-Ray Fluorescence (Nano-XRF) microscopy were performed to  
149assess the spatial distribution of the REEs in the BR. For the SEM-EDX analysis, a BR pellet  
150was prepared with 5g of BR dispersed in 25mL of ultrapure water, centrifuged at 2061xg for  
15115 minutes and dried to remove excess salts. The process was repeated 3 times. SEM was  
152carried out at 30kV using a Zeiss GeminiSEM 500 SEM equipped with an EDAX Octane  
153Silicon Drift Detector (129 eV energy resolution for Manganese) at Aix-Marseille University.  
154Nano X-Ray Fluorescence microscopy (nano-XRF) experiments were performed at the  
155Nanoscopium hard X-ray nanoprobe beamline of Soleil Synchrotron (Saint-Aubin, France).

156 Dry and washed BR was homogeneously dispersed on Kapton tape for analysis. The  
 157 monochromatic X-ray beam energy was set at 18.3 keV with a gap size of 150 x 60 nm,  
 158 focused with a Kirckpatrick-Baez nano-focusing mirror. A fast continuous scanning  
 159 technique was used to obtain elemental mapping with an integration time of 40 ms per pixel. Y  
 160 was located at the nano scale with the fluorescence K-emission line at 14.9 keV. A dead time  
 161 correction was applied to each pixel. Elemental maps were extracted from the hyperspectral  
 162 maps, including Y ( $K_{\alpha}$  14.96 keV), Fe ( $K_{\alpha}$  6.40 keV), Ti ( $K_{\alpha}$  4.51 keV), Yb ( $L_{\alpha}$  7.42 keV) and  
 163 Er ( $L_{\beta}$  7.81 keV). Elemental mapping was performed by selecting an ROI of energy centered  
 164 on the emission line on the XRF spectra using PYMCA software (background subtraction,  
 165 calibration, fit (*see S3 in SI*)). Possible correlations were further investigated by calculating  
 166 the Pearson coefficient on the nano-XRF maps.

167 **Yttrium speciation.** X-ray absorption spectra (XAS) at Y K-edge (17.038 keV) were  
 168 recorded by the P65 undulator beamline at the Deutsches Elektronen-Synchrotron (Hamburg,  
 169 Germany). Incoming photon flux energy was modulated using a Si(111) double crystal  
 170 monochromator and higher harmonics were suppressed using Rh-plane mirrors. The data were  
 171 collected in continuous mode with a beam size of 0.3 x 1.5 mm<sup>2</sup>. Samples were prepared as  
 172 pure pellets (50 mg) for BR, or as diluted pellets with polyvinylpyrrolidone for model  
 173 compounds. For the latter, the quantity of the sample was calculated to get  $\Delta\mu_{\text{theoretical}}=1$ . Each  
 174 spectrum was measured at 20 K to prevent beam damage. The BR sample was measured in  
 175 fluorescence mode with a Hitachi/Vortex 4-pixel silicon drift detector (SDD). One spectrum  
 176 represented an average of 3 to 6 scans of Y reference compounds and 30 scans of the BR  
 177 sample, depending on the concentration of Y and the noise level. Energy was calibrated using  
 178 reference Y metal foil. E0 (absorption edge) was defined at 17038 eV at the gap between the  
 179 two maximum points of the first derivative. Calibration, normalization and averaging data  
 180 were performed using Athena software <sup>14</sup>.

181 A library of Y reference compound spectra was used to identify Y species in BR. It consisted  
 182 in commercial references: yttrium oxide (Y<sub>2</sub>O<sub>3</sub>; Acros Organics), yttrium carbonate  
 183 (Y(CO<sub>3</sub>)<sub>3</sub>.xH<sub>2</sub>O; Alfa Aesar), natural minerals (xenotime, YPO<sub>4</sub>), and model compounds  
 184 synthesized in the laboratory (crystallized and amorphous Y phosphates, Y hydroxide, Y-  
 185 adsorbed on montmorillonite, (*see S4 in SI for synthesis protocols*). Least square linear  
 186 combination fitting (LCF) of the XANES (X-ray Absorption Near Edge Spectroscopy) region  
 187 was performed over an energy range of -50 eV to +200 eV around E0 using Athena software.  
 188 The residual factor of LCF was calculated as follows:  $R = (\sum(\mu_{\text{exp}} - \mu_{\text{fit}})^2) / \sum(\mu_{\text{exp}})^2$  using Athena  
 189 software. At each step of the fitting, an additional reference spectrum was added if the two

190 following conditions were true: the R factor decreased by 20% or more and the additional  
 191 reference contributed 10% or more Y species. The uncertainty of this LCF method was  
 192 estimated at  $\pm 15\%$  <sup>15</sup>.

193 **Dissolution with LMWOAs.** Three LMWOAs (citric, tartaric, and oxalic acids) and their  
 194 conjugated bases were tested. The molecular structures of LMWOAs are similar with a short  
 195 carbon chain ( $C_2-C_6$ ), carboxylic acid functions ( $-COOH$ ) and similar pKa. The complexing  
 196 reagents used were citric acid (>99%), di-hydrated trisodium citrate (99%), di-hydrated oxalic  
 197 acid (98%), mono-hydrated di-ammonium oxalate (>99%), L (+)-tartaric acid (99.5%), and  
 198 tetra-hydrated potassium tartrate (<99%). The dissolution experiments consisted in two 48-h  
 199 sequential experiments performed in triplicate at a liquid/solid ratio (L/S) of 50 (0.8g of dried  
 200 and hand-ground BR in 40ml of complexing solution at 0.1mol/L). Forty-eight hours consist  
 201 in the time needed to reach a steady-state dissolution for most elements (*see S5 in SI*). The  
 202 complexing solution was renewed 48 hours after the solid phase was separated by  
 203 centrifugation (6 133 x g). To increase the pH from 2 to 9, the organic acids used were mixed  
 204 with their conjugated base at different ratios (citric acid and citrate for example, (*see S6 in*  
 205 *SI*)). The total concentration of complexing reagents (LMWOAs and their conjugate base)  
 206 was maintained at 0.1M. During dissolution, the solutions were stirred on a Heidolph REAX  
 207 20 1-16 RPM mechanical rotary shaker (14 rpm), at room temperature. pH was measured  
 208 regularly with a HI 2550 Multiparameter pH/ORP/ $^{\circ}C$ /EC/TDS/NaCl Bench Meter. In the  
 209 literature (*see S1 in SI*), leachate is typically separated from the solid residue using 0.22 $\mu m$  or  
 210 0.45 $\mu m$  filters. Here, ultrafiltration (3kDa=1-2nm) of the leachate insured that there were no  
 211 suspended particles in the solution by separating only dissolved species or small organic-  
 212 metal complexes. The filtered solutions were diluted by a factor of 20 or 40 and analyzed  
 213 using both ICP-OES and ICP-MS.

214 The results are presented with their dissolution percentage (concentration of the dissolved  
 215 element in mg/kg divided by the concentration in the BR in mg/kg, converted into  
 216 percentage). Selectivity was calculated with the enrichment factor (EF) according to the  
 217 following equation:

$$218 \quad EF = \frac{\sum [REEs](dissolved)}{\sum [Fe, Al, Ti](dissolved)} \cdot \frac{\sum [REEs](BR)}{\sum [Fe, Al, Ti](BR)} \quad (\text{Equation 1})$$

Where *dissolved* stands for the concentrations of element in the filtered solution (mg/kg) and *BR* for the concentrations of the element in the original material (mg/kg). EF stands for the enrichment of REEs, Y and Sc in the 3 most concentrated elements (Fe, Al, Ti) in BR.

**Dissolution with nitric acid.** A dissolution experiment with a mineral acid was performed for comparison with ligand-promoted dissolution. Two concentrations of HNO<sub>3</sub> (0.1M, 0.05M) were used to target low and close to neutral pH (pH<sub>mix</sub>=2 and 5.3 respectively). The dissolution protocol used was the same as that used for dissolution with LMWOAs described above.

## Results and discussion

### Characterization of initial BR

### Chemical composition and mineralogy

The chemical composition and the mineralogy of BR is presented in *Table 1* and in SI (S7). BR was mainly composed of Fe (33wt%), in the form of hematite ( $\alpha$ -Fe<sub>2</sub>O<sub>3</sub>) and goethite ( $\alpha$ -FeOOH) followed by Ti (5.41wt%) as rutile (TiO<sub>2</sub>) and Al (3.91wt%) as gibbsite (Al(OH)<sub>3</sub>). Calcium is present as calcite (CaCO<sub>3</sub>). Two silicate phases were identified: cancrinite (Na<sub>6</sub>Ca<sub>2</sub>CO<sub>3</sub>, Al<sub>6</sub>Si<sub>6</sub>O<sub>24</sub>·2H<sub>2</sub>O) and katoite (Ca<sub>3</sub>Al<sub>2</sub>(SiO<sub>4</sub>)<sub>3-x</sub>(OH)<sub>4x</sub>, x=1.5 to 3). This is consistent with the literature on BR composition and mineralogy: Fe and Al are usually the two main concentrated elements, but their concentration varies considerably depending on the origin, the type of the bauxite (lateritic or karstic)<sup>7,16</sup>, the Al extraction treatment conditions (pH, temperature, reagents) and the storage time<sup>17,18</sup>. Together, reviews<sup>17,19,20</sup> by *Xue et al.* 2016, *Gräfe, Power, and Klauber* 2011 and *Snars and Gilkes* 2009, and the estimation by the International Aluminum Institute (IAI) and the European Aluminum Association (EAA) in 2014, suggest that Fe<sub>2</sub>O<sub>3</sub> comprises from 7% to 72wt% of the residue, Al<sub>2</sub>O<sub>3</sub> 2% to 33wt%, TiO<sub>2</sub> 1% to 23 wt%, CaO 0% to 14 wt% and SiO<sub>2</sub> 5% to 30 wt%. Aside from Al and Fe, the mineralogy we observed is consistent with the literature<sup>17</sup>. Other inorganic phases reported in other studies including perovskite (CaTiO<sub>3</sub>), sodalite (Na<sub>4</sub>(Si<sub>3</sub>Al<sub>3</sub>)O<sub>12</sub>Cl), diasporite (AlO(OH)) or magnetite (Fe<sub>3</sub>O<sub>4</sub>) were not detected in our BR sample<sup>21,22</sup>.

The total amount of REEs, including Y and Sc in the BR studied here was 712.6mg/kg. The most concentrated REEs were Ce (220.7mg/kg), Y (121.2mg/kg), La (105.9mg/kg) and Sc (75.2mg/kg). The concentration of REEs in BR reported in the literature is highly variable (see S8 in SI). The main variations in the concentration of REEs are explained by the origin of



the bauxite deposit: karstic-type bauxites (12% of the global bauxite deposits mostly located in Europe) are usually richer in REEs than lateritic-type bauxites (88% of the global bauxite that can be found in Guinea, India or Australia for example). In this study, the BR was produced from a lateritic deposit (in Guinea, West Africa) using the Bayer process. No particular anomalies were observed according to the PAAS-normalized REE pattern (see S9 in SI).

258

**Table 1 : Chemical composition of the BR for REEs, Sc, Y, and major elements (average  $\pm$  standard deviation). Concentrations in the Earth's crust were taken from Kabata-Pendias 2011.**

REEs	BR Concentration (mg/kg DW)	Earth's crust (mg/kg DW)
Sc	75.2 $\pm$ 1.7	16-30
La	105.9 $\pm$ 2.0	30
Ce	220.7 $\pm$ 3.2	60
Pr	21.0 $\pm$ 0.3	8.2
Nd	72.1 $\pm$ 0.9	28
Sm	16.7 $\pm$ 0.2	4.7
Eu	3.1 $\pm$ 0.1	1.2
Gd	16.7 $\pm$ 0.2	5.4
Tb	3.1 $\pm$ 0.1	0.6
Dy	21.3 $\pm$ 0.4	3.7
Ho	4.6 $\pm$ 0.1	0.8
Er	14.4 $\pm$ 0.5	2.8
Tm	2.2 $\pm$ 0.1	0.5
Yb	15.2 $\pm$ 0.3	2.2
Lu	2.3 $\pm$ 0.1	0.3
Y	121.2 $\pm$ 3.0	20-33
<i>Total REEs</i>	<b>712.6<math>\pm</math>13.1</b>	168-200

Majors	Mass (%)	Equivalent oxide (%)
Fe	33.03 $\pm$ 0.61	47.22 $\pm$ 0.87 (Fe <sub>2</sub> O <sub>3</sub> )
Ti	5.41 $\pm$ 0.05	9.02 $\pm$ 0.08 (TiO <sub>2</sub> )
Al	3.91 $\pm$ 0.23	7.39 $\pm$ 0.43 (Al <sub>2</sub> O <sub>3</sub> )
Ca	2.95 $\pm$ 0.20	4.13 $\pm$ 0.28 (CaO)
Si	1.43 $\pm$ 0.12	3.06 $\pm$ 0.26 (SiO <sub>2</sub> )
P	0.17 $\pm$ 0.02	0.77 $\pm$ 0.07 (PO <sub>4</sub> )

262

263

264

#### Spatial distribution of REEs in BR

17

18

Elemental mapping with SEM-EDX confirmed the prevalence of Fe in our BR matrix (Figure 1A). Discrete particles rich in Al (dark blue), Si (red), Ti (pink) and Ca (cyan) were also observed confirming the results of bulk analysis and the mineralogy observed by XRD. The detection of REEs was very challenging because of (i) their relatively low concentration (especially HREEs), and (ii) the overlap between their  $L_{\alpha}$  fluorescence emission lines with the  $K_{\alpha}$  emission lines of Ti, Cr and Fe (regarding LREEs). However, few Y-rich particles (white) were observed with SEM-EDX (Figure 1A). Y was not correlated with Al, Fe, Ti, Si and Ca but co-localized with P (light blue). This co-localization raises the hypothesis that Y and P could exist as yttrium phosphates ( $YPO_4$ ). Indeed, Y commonly occurs in phosphate minerals (such as monazite, xenotime) in nature and forms very stable phases. At this stage, no other REEs were detected by SEM-EDX.

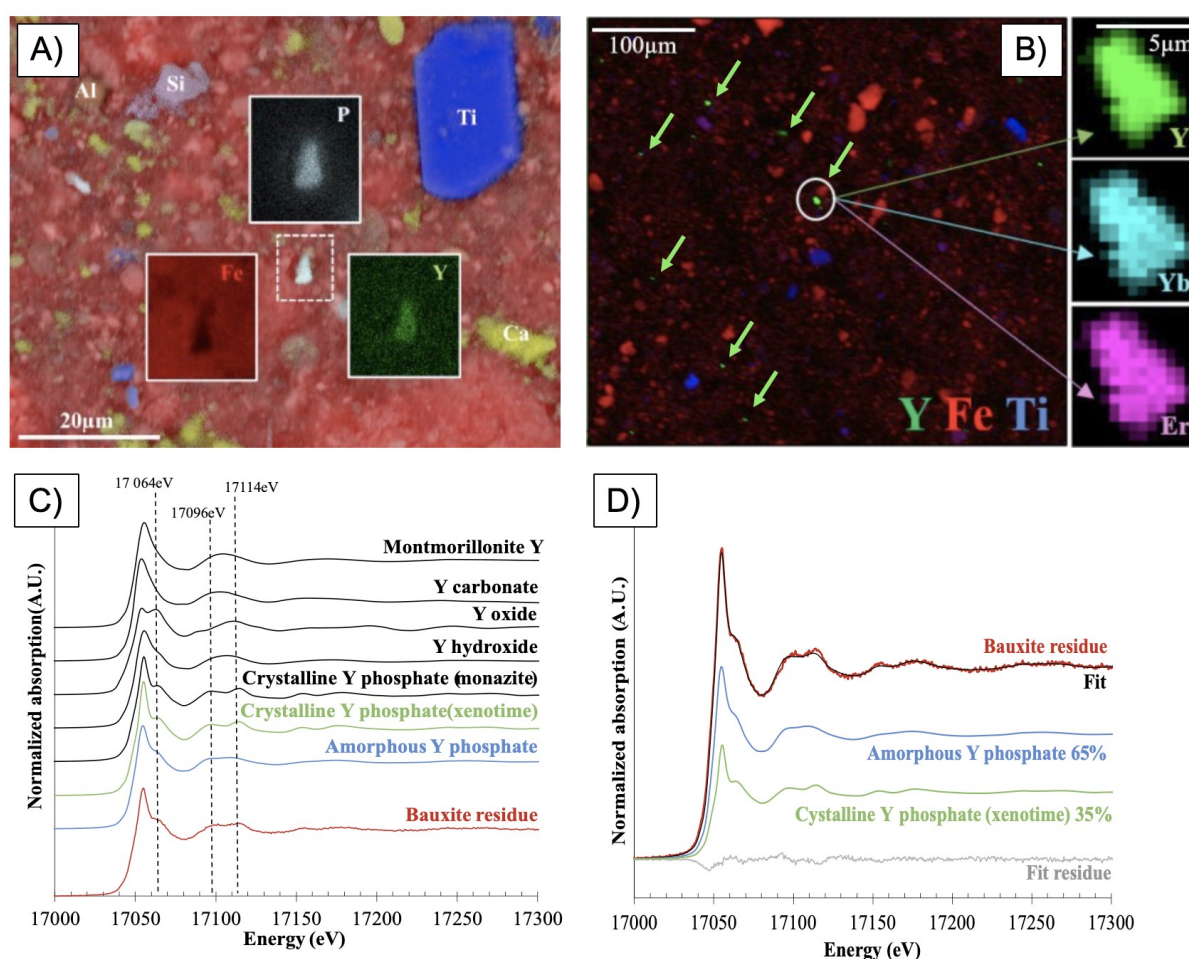


**Figure 1:** (A) Combined elemental map obtained by SEM-EDX showing the spatial correlation between Al, Si, Ti, Fe, Ca, Y and P in BR sample (30kV, pixel=71.11nm). (B) Combined elemental map obtained by nano-XRF showing the distribution of Fe, Ti, Y, Yb, Er in BR sample, (1px = 1 μm for the large image, 1px = 400nm for small images). (C)

**Bulk XANES spectra of BR and model compounds at the Y K-edge and (D) LCF performed with Athena software (R-factor=0.0009)(right).**

285

286 Deeper investigation of the spatial distribution was performed at the SOLEIL synchrotron  
287 with using nano-XRF which is more sensitive than that of SEM-EDX. In agreement with  
288 SEM, nano-XRF revealed several Y-rich particles (*Figure 1B*) of  $4.9 \pm 1.9 \mu\text{m}$  ( $n=24$ ) not  
289 associated with major elements (Fe, Ti, Al, Si, Ca) but co-localized with other REEs,  
290 especially HREEs, as expected (Gd, Er, Yb). LREEs (La, Ce, Nd) were also investigated but  
291 were not detected, probably because their signals are hidden by the intense XRF emissions of  
292 Ti, Cr and Fe. P was not detected either because of the limited sensitivity of the beamline for  
293 the detection of P K $\alpha$  emission lines. At this low energy (2.01 keV), fluorescence signal is  
294 strongly absorbed by the air before reaching the detector, unlike in SEM-EDX analysis, which  
295 is performed under vacuum.

296 The Pearson coefficient was calculated for some trace elements (Y, Yb, Gd, Er, Cu, U, Th)  
297 and for major elements (Fe, Ti) on the Y-rich area (Inset in *Figure 1B*) (*Figure S2, SI*). A  
298 correlation was observed (Coef  $\geq 0.70$ ) for the HREEs (Gd, Er, Yb) and Y, but also for other  
299 elements of interest present at low concentrations such as Cu, U and Th. Fe and Ti were not  
300 correlated with these elements. To confirm our hypothesis that Y forms YPO<sub>4</sub> phases,  
301 probably associated with HREEs in BR, Y speciation was investigated at the bulk scale.

302

### 303 **Y speciation in BR**

304 The bulk XAS spectrum (*Figure 1C*) obtained for the BR sample closely resembled spectra  
305 corresponding to synthesized Y phosphates (amorphous and crystallized monazite), and  
306 xenotime (natural and crystalline phosphate mineral). The spectra of these model compounds  
307 were characterized by specific features, i.e., a shoulder at 17064 eV in the white line and the 2  
308 features at 17096 eV and 17114 eV. The amorphous Y phosphate had less pronounced features.  
309 Linear combination fitting (LCF) confirmed that the Y speciation in BR was YPO<sub>4</sub> (*Figure*  
310 *1D*) in agreement with the Y/P spatial correlation previously identified with SEM-EDX. The  
311 best fit was obtained using a mixture of crystalline and amorphous YPO<sub>4</sub> (35% xenotime and  
312 65% amorphous).

313 These results concerning HREEs are consistent with those obtained in the study by *Vind and al.*  
314 (2018)<sup>16</sup> where Y, Gd, Dy and Er were found to be co-localized at the particle scale using an  
315 Electron Probe Micro Analyzer (EPMA) and EDX methods as xenotime/churchite-kind phases  
316 (yttrium phosphate). Observed in a karstic BR, these microscale particles were slightly smaller

317(2-3µm) than the ones observed in our study. Our study thus confirms for the first time at the  
318bulk scale, observations performed at small scale. It is likely that we only observed the biggest  
319particles and missed a large fraction of sub-micron particles, potentially amorphous (1µm pixel  
320on the big map in *Figure 1B*). The distributions of REEs and Y observed here as well as by  
321Vind and al. (2018)<sup>16</sup> confirm that BR is potentially an ideal matrix for developing selective  
322dissolution of HREEs since it is concentrated in accessible particles and not associated with  
323major elements.

324

## 325Dissolution of REEs using LWMOAs

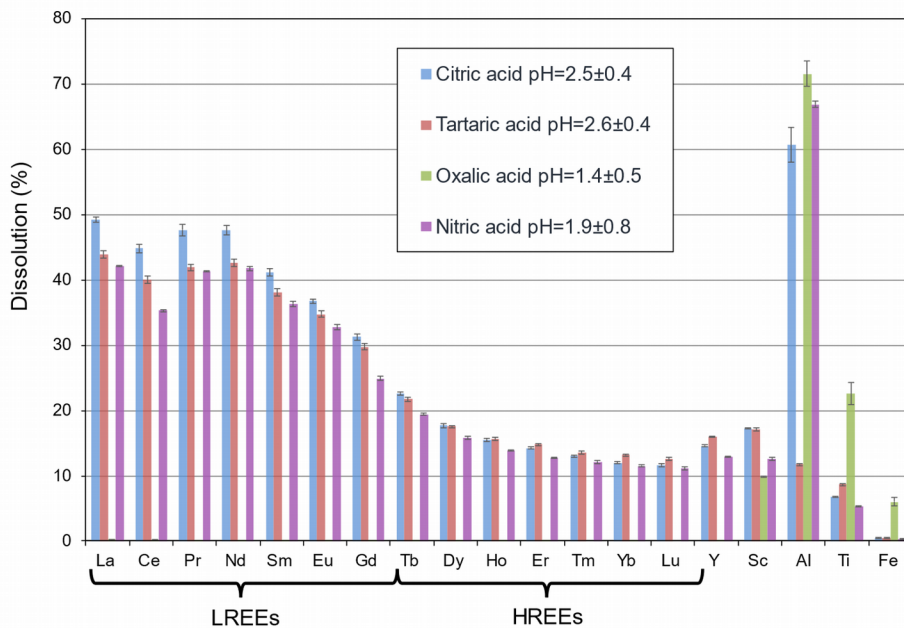
### 326Ligand-dependent dissolution

327It has been shown that aliphatic acids (citric acid, oxalic acid, succinic acid, malic acid, etc.)  
328produced by organisms such as plants, fungi and bacteria are good candidates for the recovery  
329of REEs from REEs/Y-rich phosphate minerals (apatite and monazite), particularly citric acid  
330<sup>23-25</sup>. Some of these organic acids have also been identified in the literature as biomolecules  
331capable of selectively solubilizing REEs from BR (*Table S1, SI*).

332Figure 2 shows the fraction of dissolved elements (REEs, Y, Sc and major elements Al, Ti, Fe)  
333after two-step sequential extraction (2x48 h) for three organic acids that have known affinity  
334for REEs (citric, tartaric, and oxalic acids) and nitric acid. Citric and tartaric acids exhibit  
335quite similar behavior that is very different from that of oxalic acid. Citric acid dissolves more  
336LREEs and Al. It can extract up to 49% of LREEs and 12% of HREEs. Tartaric acid dissolves  
337slightly more HREEs, Y, Sc, Ti and Fe. More interestingly, it dissolves Al poorly in  
338comparison with citric acid, which might be of interest in terms of selectivity. This can be  
339explained by the lower affinity of tartrate for Al compared to citrate (log K= 5.32 and 7.98  
340respectively). Finally, no REEs were measured in solution in the oxalic acid experiment,  
341unlike Al, Ti, Sc, and a small amount of Fe. This was not surprising since oxalic acid is often  
342used in industrial processes to precipitate the REEs as insoluble metal-oxalate complexes<sup>26-29</sup>.  
343In our study, it was not possible to quantify the amount of REEs that reacted with oxalic acid.  
344In the citric and tartaric acid systems, LREEs (La to Sm) were better dissolved than HREEs  
345(Ho to Lu, Y and Sc) and the dissolution of Eu to Dy was intermediate. Two hypotheses may  
346explain this trend: (i) the stability constants of ligand-REEs complexes are lower for HREEs  
347than for LREEs for a given speciation, (ii) LREEs and HREEs have different speciation and  
348consequently different affinities for the extractant. The second hypothesis is more likely, in  
349view of the speciation data collected in our study and in the study by Vind and al. (2018)<sup>16</sup>. In  
350addition, stability constants reported in the literature show either a continuous increase with Z

351or close values for LREEs and HREEs (see S10 in SI)<sup>30,31</sup>, which is not consistent with our  
352first hypothesis.

353For the sake of comparison, a similar experiment was performed using nitric acid. Nitric acid  
354is usually described in the literature as one of the most efficient inorganic lixiviants for  
355leaching of REEs from BR under very acidic conditions (pH<0.5)<sup>10,11,32</sup>. At pH 1.9±0.8 (0.1M  
356HNO<sub>3</sub>), the recovery yields were slightly lower but close to those obtained with citric and  
357tartaric acids at pH=2.5±0.4 and 2.6±0.4. We hypothesize that at these relatively low pH,  
358proton-promoted dissolution is the dominant mechanism for the dissolution of REEs.  
359However, in the presence of LMWOAs, ligand-promoted dissolution is also probably  
360involved in the dissolution of LREEs, which may explain the slightly better dissolution  
361efficiency of REEs by citric and tartaric acids compared to HNO<sub>3</sub> treatment. However, at this  
362stage, it is difficult to dissociate the two mechanisms taking place with LMWOAs. The  
363potential effect of the ligand-promoted dissolution was studied by performing similar  
364experiments at higher pH at which proton-promoted dissolution is negligible.



365

366**Figure 2 : Dissolution of REEs, Fe, Al and Ti with citric acid, tartaric acid, oxalic acid, and**  
367**nitric acid (2x48 h, 0.1mol/L, L/S=50).**

### 368pH-dependent dissolution

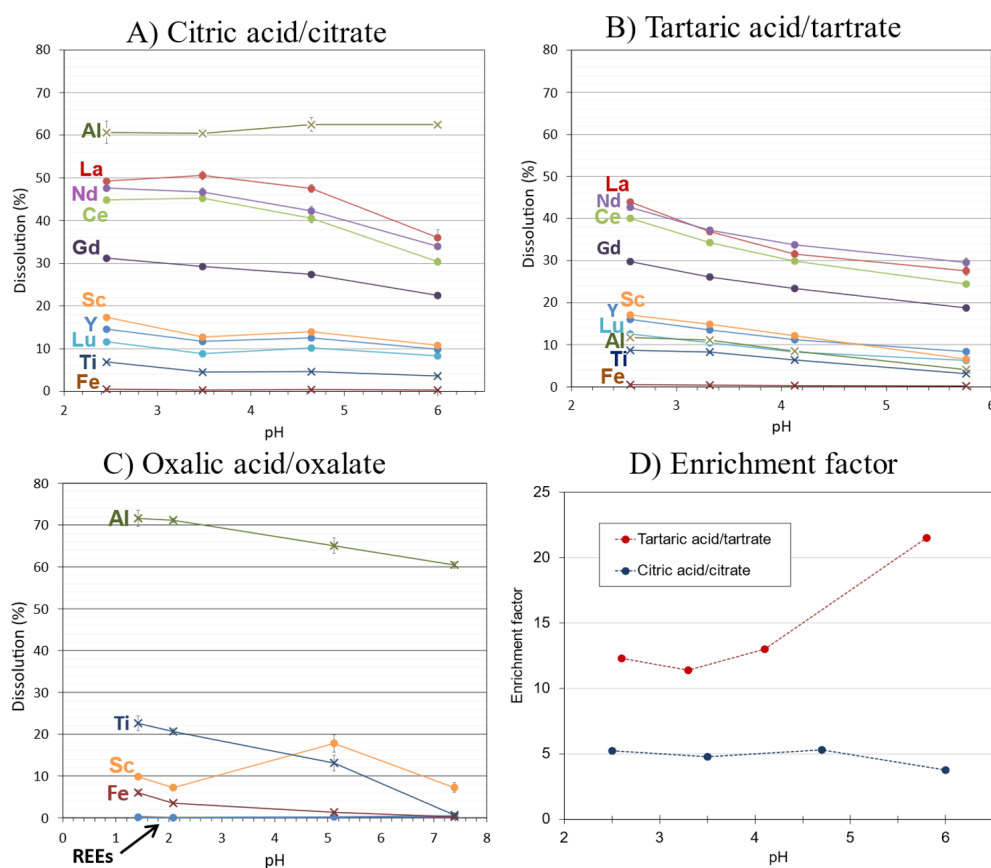
369To further decipher the role of ligand-promoted dissolution, a set of dissolution experiments  
370was performed at different pH. pH was controlled by varying the acid/conjugate base ratio.

371The better dissolution of LREEs compared to HREEs observed above at pH 2.5 with citric  
372acid and at 2.6 with tartaric acid was also observed at all the pH tested using the citric  
373acid/citrate and tartaric acid/tartrate systems.

374Regarding the citric acid/citrate system, similar dissolution was obtained from pH 2.5 to 4.7  
375before a significant drop at pH 6 (*Figure 3A*). The average dissolution of Al is 61%, with low  
376variability among the pH range investigated here. Ti and Fe dissolution were low (%Ti<6%,  
377%Fe<1%) and decreased toward alkaline pH.

378The tartaric acid/tartrate system behaved differently from the citric acid/citrate system with a  
379decrease in the dissolution of REEs with increasing pH (*Figure 3B*). However, the major  
380elements including Al were poorly dissolved compared to in the citric acid/citrate system. Al  
381dissolution did not exceed 12% (pH=2.6±0.4), only 9% of Ti, and less than 0.5% of Fe were  
382dissolved.

383As mentioned earlier, oxalic acid is known in the literature as an efficient complexing and  
384precipitating agent for REEs at acidic pH <sup>26–29</sup>. Consequently, no REEs or Y dissolution was  
385measured (*Figure 3C*) regardless of the pH in the oxalic acid/oxalate system  
386(%REE,Y<0.5%). A fraction of REEs probably precipitated with oxalate and was therefore  
387not detected in the supernatant. Interestingly, Sc was partly dissolved with optimal extraction  
388at pH=5.1±1.6 (%Sc=18%) which confirms the difference in the chemical behavior of this  
389element from that of other REEs. Between 60% and 70% of the Al was dissolved at pH< 7.5  
390and Ti dissolution increased from 13% at pH=5.1±1.6 to 22% at pH=1.4. More Fe was more  
391dissolved with oxalic acid than with the other organic ligands (%Fe>3.5% for pH<2).



392

393 **Figure 3 : Dissolution of REEs, Sc, Y, Al, Ti, and Fe with (A) citric acid/citrate, (B) tartaric**  
 394 **acid/tartrate, and (C) oxalic acid/oxalate as a function of pH (2x48h, L/S=50, 0.1mol/L).**  
 395 **(D) Selectivity (expressed by the enrichment factor) for the dissolution with citric**  
 396 **acid/citrate and tartaric/tartrate acid.**

397 Although less efficient at mild pH than the citric acid/citrate system, the tartaric acid/tartrate  
 398 system is interesting in terms of selectivity, especially related to Al. To quantify the selectivity  
 399 of REE dissolution, an enrichment factor (EF) towards the 3 main elements was calculated  
 400 (Figure 3D). Despite slightly lower recovery yields, tartaric acid was found to be more  
 401 selective for REEs than citric acid regardless of the pH:  $EF_{\text{citric acid}}=3.8$  to  $5.3$  and  $EF_{\text{tartaric}}$   
 402  $_{\text{acid}}=11.4$  to  $21.5$  for  $2.5 < \text{pH} < 6$ . The enrichment factor was similar regardless of the pH, except  
 403 at  $\text{pH}=6$  for tartaric acid where selectivity reached maximum.

404

#### 405 **Dissolution mechanisms**

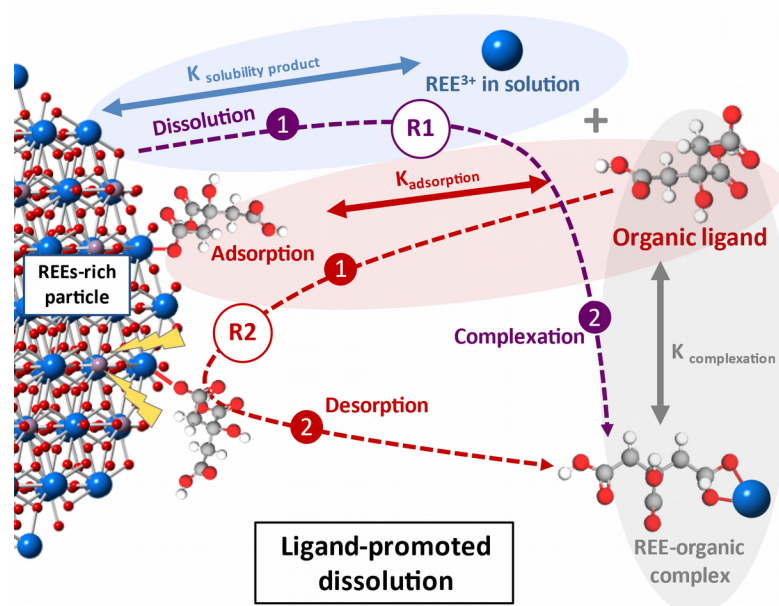
406 To better understand the mechanisms involved as a function of pH, recovery yields were  
 407 measured using  $\text{HNO}_3$  at 0.05M to reach a pH of 5.3 (see S11 in SI). In this condition, there  
 408 was no dissolution of REEs, Y or Sc unlike in the citric/citrate and tartaric/tartrate systems at



409 similar pH. This experiment confirms that at such mild pH, ligand-promoted dissolution is the  
410 main driver of the dissolution of REEs.

411 Two routes for ligand-promoted dissolution may exist, as illustrated in *Figure 4*. Based on the  
412 observations we made in this study for HREEs, we hypothesize that HREEs are hosted in a  
413 phosphate matrix. LREEs on the other hand are suspected to be concentrated within particles  
414 with varying chemistries <sup>16</sup>. The first route (R1 in *Figure 4*) is controlled by (i) the dissolution  
415 of the REE-hosting mineral defined by the solubility product constant  $K_{sp}$  and (ii) the affinity  
416 of the dissolved species for the organic ligand defined by the complexation constant  
417  $K_{complexation}$ . The complexation of free  $REE^{3+}$  ion by organic ligands will shift the first  
418 equilibrium towards dissolution of REE-hosting mineral.

419 The second route (R2 in *Figure 4*) is controlled by the affinity of the organic ligand for the  
420 surface of the REE-hosting mineral present in BR ( $K_{adsorption}$ ) and its ability to weaken the  
421 bonds that bind surface atoms to the particle and that will eventually break to form a complex  
422 in solution.



423

424 **Figure 4 : Conceptual diagram of the chemical mechanisms involved in the dissolution of**  
425 **REEs in bauxite residues with organic ligands.**

426 As a result of these processes, dissolution may be affected by a number of parameters  
427 including the solubility product of the different phases that comprise the BR, the affinity of  
428 the LMWOAs for soluble REEs and particle surfaces. For the latter, pH is a key parameter  
429 that controls the dissociation of LMWOA protons (pKa) and the surface charge of the mineral.



Therefore, improving dissolution efficiency requires a good understanding of dissolution mechanisms, which, in turn requires a good knowledge of the physico-chemical properties of the matrix. To give an example, the poor dissolution of HREEs in our case could be explained by their speciation. The REE-phosphates observed in our study are known to be very stable (poorly soluble,  $K_{sp}=10^{-24.75}$  to  $10^{-26.43}$  for REEs and Y)<sup>33</sup> which will limit dissolution (route 1) and prevent the release of the REE-organic ligand complex (route 2). Further improvement of the process for HREEs should focus on identifying other organic ligands that have a high affinity for phosphate minerals (either for the HREEs or for the phosphate function) in order to favor route 2 since route 1 seems unfavorable in the presence of REE-phosphate (*Figure 4*). The better dissolution yield of LREEs compared to HREEs was probably due to the occurrence of LREEs phases that are less chemically stable (e.g. higher solubility product (route 1) or less energetic release of REE-organic ligand complex (route 2)) than the HREEs-phosphates observed in our study. Although the speciation of LREEs seems to differ from that of HREEs<sup>16</sup>, the host LREEs-phases are still not known, and work is now underway to characterize it.

## Conclusion

Rather than focusing on maximum dissolution efficiency, which is the primary objective of past studies on the dissolution of REEs from BR, our study aimed at investigating the potential of ligand-promoted dissolution for the selective dissolution of REEs under mild pHs. In the citric acid/citrate system, similar recovery yields were obtained at pH ranging from 2.5 to 4.7. Although slightly less efficient, the tartaric acid/tartrate system displayed interesting dissolution selectivity with enrichment factors comparable to those of Al, Fe and Ti reaching up to 21.5. Unlike in strong mineral acid, it is therefore possible to dissolve REEs at mild pH with relatively good selectivity.

Understanding ligand-promoted dissolution mechanisms in the optic of improving the efficiency and selectivity of REE dissolution requires a good knowledge of the BR matrix, which was investigated in our study. LREEs were recovered better than HREEs most probably because of the difference in speciation in the BR. Yttrium was found as  $4.9\ \mu\text{m}$   $\text{YPO}_4$  particles. HREEs co-localized with Y and, given the analogy between Y and HREEs, the latter probably form mixed phosphate phases. Although the formation of discrete particles of Y and HREEs appears favorable for selective dissolution, the very high chemical stability

463of these phosphate phases probably explains the poor recovery yields of Y and HREEs. LREE  
464speciation is still not clear, although the literature reports LREEs (La, Ce, Nd) embedded in  
465ferrotitanate phases, and minor amounts in carbonate and phosphate phases <sup>16</sup>. Despite  
466measurement challenges, work is now underway to identify the LREE-bearing phases. In any  
467case, we hypothesize that their speciation is more favorable for their recovery using  
468LMWOAs. The case of Sc is probably not favorable for selective dissolution since it has been  
469shown to be strongly associated with iron phases <sup>4</sup>. As an example, in a previous study, we  
470showed that Sc can replace Fe in the goethite structure making dissolution selectivity  
471impossible to address for this element <sup>4</sup>.

472Several options will be investigated in future studies to improve dissolution efficiency and  
473selectivity, in particular for HREEs. One possibility is to favor route 2 of the mechanisms  
474described in *Figure 4* by selecting appropriate organic ligands that have a stronger affinity for  
475REE-rich phases than the LMWOAs tested in the present study. In this regard, understanding  
476the effect of ligand composition and structure (e.g. nature and number of functional groups,  
477the presence of an hydroxyl group in  $\alpha$ -,  $\beta$ - or  $\gamma$ -hydroxy acids, pKas, etc.) on the dissolution  
478of REE-rich phases can help in the choice of more appropriate ligands in the optic of  
479enhanced dissolution yield and selectivity. In addition, the use of organic molecules produced  
480by living organisms will also be explored. It includes highly selective organic molecules  
481produced specifically to recover REEs by methylotroph bacteria such as lanmodulin <sup>34–36</sup> but  
482also other molecules produced by plants, bacteria or fungi than are known to dissolve  
483phosphates and/or REEs in soil (siderophores <sup>37–39</sup>, formic acid, succinic acid, malic acid,  
484amino acids...) <sup>23,25,40–46</sup>. In this regard a better knowledge of plants and microorganisms  
485developing in BR deposits may be particularly informative for selecting appropriate bio-  
486inspired extraction strategies<sup>47–49</sup>.

487

488Although poorly investigated compared to conventional hydrometallurgy, we believe that  
489selective dissolution using ligand-promoted dissolution is a promising approach for the design  
490of sustainable extraction processes of various critical elements from a variety of secondary  
491sources. In a circular economy, this approach makes it possible to decrease pressure on natural  
492resources, to limit the number of extraction steps and to minimize the production of hazardous  
493wastes.

494

495**Supplementary information:** Complementary literature, additional experimental details  
496including synthesis protocols, additional results including XRF spectra analysis, granulometry  
497experiments and nitric acid dissolution. The document is available online.

498

#### 499**Acknowledgments**

500The authors acknowledge financial support from the CNRS through the MITI  
501interdisciplinary programs (PRIME 2020: ExtraMet project), the Agence Nationale de la  
502Recherche through the RECALL project (ANR-20-CE04-0007). This work was supported by  
503the TelluS Program of CNRS/INSU as well as in the framework of the OHM Bassin Minier de  
504Provence and (co)funded by the LabEx DRIIHM, French program “*Investissements d’Avenir*”  
505(ANR-11-LABX-0010) managed by the ANR. The thesis contract of C. Lallemand was  
506funded by CEPAC (*Caisse d’épargne* Provence Alpes Corse) through the AMIDEX  
507foundation (Aix-Marseille University). Synchrotron data were obtained on SOLEIL and  
508DESY synchrotrons. We are very grateful to the SOLEIL beamline staff for their assistance, in  
509particular to Andrea Somogyi (Nanoscopium). We also acknowledge DESY (Hamburg,  
510Germany), a member of the Helmholtz Association HGF, for the use of experimental  
511facilities. Parts of this research were carried out at P65.

512

## REFERENCES

- 514(1) European Commission, Study on the EU's List of Critical Raw Materials - Final Report  
515 (2020).
- 516(2) Jowitt, S. M.; Werner, T. T.; Weng, Z.; Mudd, G. M. Recycling of the Rare Earth  
517 Elements. *Current Opinion in Green and Sustainable Chemistry* **2018**, *13*, 1–7.  
518 <https://doi.org/10.1016/j.cogsc.2018.02.008>.
- 519(3) *Environmental Technologies to Treat Rare Earth Elements Pollution: Principles and*  
520 *Engineering*; Sinharoy, A., Lens, P. N. L., Eds.; IWA Publishing, 2022.  
521 <https://doi.org/10.2166/9781789062236>.
- 522(4) Levard, C.; Borschneck, D.; Grauby, O.; Rose, J.; Ambrosi, J.-P. Goethite, a Tailor-  
523 Made Host for the Critical Metal Scandium: The FeSc(1-x)OOH Solid Solution.  
524 *Geochem. Persp. Let.* **2018**, 16–20. <https://doi.org/10.7185/geochemlet.1832>.
- 525(5) Mancheri, N. A. Effect of Chinese Policies on Rare Earth Supply Chain Resilience.  
526 **2019**, 12.
- 527(6) Golev, A.; Scott, M.; Erskine, P. D.; Ali, S. H.; Ballantyne, G. R. Rare Earths Supply  
528 Chains: Current Status, Constraints and Opportunities. *Resources Policy* **2014**, *41*, 52–  
529 59. <https://doi.org/10.1016/j.resourpol.2014.03.004>.
- 530(7) Binnemans, K.; Jones, P. T.; Blanpain, B.; Van Gerven, T.; Pontikes, Y. Towards Zero-  
531 Waste Valorisation of Rare-Earth-Containing Industrial Process Residues: A Critical  
532 Review. *Journal of Cleaner Production* **2015**, *99*, 17–38.  
533 <https://doi.org/10.1016/j.jclepro.2015.02.089>.
- 534(8) Kabata-Pendias, A. *Trace Elements in Soils and Plants*, 4th ed.; CRC Press: Boca  
535 Raton, 2011.
- 536(9) Abhilash; Sinha, S.; Sinha, M. K.; Pandey, B. D. Extraction of Lanthanum and Cerium  
537 from Indian Red Mud. *International Journal of Mineral Processing* **2014**, *127*, 70–73.  
538 <https://doi.org/10.1016/j.minpro.2013.12.009>.
- 539(10) Ochsenkühn-Petropoulou, M. Th.; Hatzilyberis, K. S.; Mendrinos, L. N.; Salmas, C. E.  
540 Pilot-Plant Investigation of the Leaching Process for the Recovery of Scandium from  
541 Red Mud. *Ind. Eng. Chem. Res.* **2002**, *41* (23), 5794–5801.  
542 <https://doi.org/10.1021/ie011047b>.
- 543(11) Borra, C. R.; Pontikes, Y.; Binnemans, K.; Van Gerven, T. Leaching of Rare Earths  
544 from Bauxite Residue (Red Mud). *Minerals Engineering* **2015**, *76*, 20–27.  
545 <https://doi.org/10.1016/j.mineng.2015.01.005>.
- 546(12) Qu, Y.; Lian, B. Bioleaching of Rare Earth and Radioactive Elements from Red Mud  
547 Using Penicillium Tricolor RM-10. *Bioresource Technology* **2013**, *136*, 16–23.  
548 <https://doi.org/10.1016/j.biortech.2013.03.070>.
- 549(13) Borra, C. R.; Blanpain, B.; Pontikes, Y.; Binnemans, K.; Van Gerven, T. Recovery of  
550 Rare Earths and Other Valuable Metals From Bauxite Residue (Red Mud): A Review. *J.*  
551 *Sustain. Metall.* **2016**, *2* (4), 365–386. <https://doi.org/10.1007/s40831-016-0068-2>.
- 552(14) Ravel, B.; Newville, M. ATHENA, ARTEMIS, HEPHAESTUS: Data Analysis for X-  
553 Ray Absorption Spectroscopy Using IFEFFIT. *J Synchrotron Rad* **2005**, *12* (4), 537–  
554 541. <https://doi.org/10.1107/S0909049505012719>.
- 555(15) Doelsch, E.; Basile-Doelsch, I.; Rose, J.; Masion, A.; Borschneck, D.; Hazemann, J.-L.;  
556 Saint-Macary, H.; Bottero, J.-Y. New Combination of EXAFS Spectroscopy and  
557 Density Fractionation for the Speciation of Chromium within an Andosol. *Environ. Sci.*  
558 *Technol.* **2006**, *40* (24), 7602–7608. <https://doi.org/10.1021/es060906q>.
- 559(16) Vind, J.; Malfliet, A.; Blanpain, B.; Tsakiridis, P.; Tkaczyk, A.; Vassiliadou, V.; Panias,  
560 D. Rare Earth Element Phases in Bauxite Residue. *Minerals* **2018**, *8* (2), 77.  
561 <https://doi.org/10.3390/min8020077>.

- 562(17) Gräfe, M.; Power, G.; Klauber, C. Bauxite Residue Issues: III. Alkalinity and  
563 Associated Chemistry. *Hydrometallurgy* **2011**, *108* (1–2), 60–79.  
564 <https://doi.org/10.1016/j.hydromet.2011.02.004>.
- 565(18) Cusack, P. B.; Courtney, R.; Healy, M. G.; O’ Donoghue, L. M. T.; Ujaczki, É. An  
566 Evaluation of the General Composition and Critical Raw Material Content of Bauxite  
567 Residue in a Storage Area over a Twelve-Year Period. *Journal of Cleaner Production*  
568 **2019**, *208*, 393–401. <https://doi.org/10.1016/j.jclepro.2018.10.083>.
- 569(19) Xue, S.; Zhu, F.; Kong, X.; Wu, C.; Huang, L.; Huang, N.; Hartley, W. A Review of the  
570 Characterization and Revegetation of Bauxite Residues (Red Mud). *Environ Sci Pollut*  
571 *Res* **2016**, *23* (2), 1120–1132. <https://doi.org/10.1007/s11356-015-4558-8>.
- 572(20) Snars, K.; Gilkes, R. J. Evaluation of Bauxite Residues (Red Muds) of Different  
573 Origins for Environmental Applications. *Applied Clay Science* **2009**, *46* (1), 13–20.  
574 <https://doi.org/10.1016/j.clay.2009.06.014>.
- 575(21) Atasoy, A. An Investigation on Characterization and Thermal Analysis of the Aughinish  
576 Red Mud. *J Therm Anal Calorim* **2005**, *81* (2), 357–361.  
577 <https://doi.org/10.1007/s10973-005-0792-5>.
- 578(22) Samal, S.; Ray, A. K.; Bandopadhyay, A. Proposal for Resources, Utilization and  
579 Processes of Red Mud in India — A Review. *International Journal of Mineral*  
580 *Processing* **2013**, *118*, 43–55. <https://doi.org/10.1016/j.minpro.2012.11.001>.
- 581(23) Goyne, K. W.; Brantley, S. L.; Chorover, J. Rare Earth Element Release from  
582 Phosphate Minerals in the Presence of Organic Acids. *Chemical Geology* **2010**, *278* (1–  
583 2), 1–14. <https://doi.org/10.1016/j.chemgeo.2010.03.011>.
- 584(24) Brisson, V. L.; Zhuang, W.-Q.; Alvarez-Cohen, L. Bioleaching of Rare Earth Elements  
585 from Monazite Sand: Bioleaching of Rare Earth Elements from Monazite. *Biotechnol.*  
586 *Bioeng.* **2016**, *113* (2), 339–348. <https://doi.org/10.1002/bit.25823>.
- 587(25) Shan, X.; Wang, H.; Zhang, S.; Zhou, H.; Zheng, Y.; Yu, H.; Wen, B. Accumulation and  
588 Uptake of Light Rare Earth Elements in a Hyperaccumulator *Dicropeteris Dichotoma*.  
589 *Plant Science* **2003**, *165* (6), 1343–1353. <https://doi.org/10.1016/S0168->  
590 [9452\(03\)00361-3](https://doi.org/10.1016/S0168-9452(03)00361-3).
- 591(26) Chi, R.; Xu, Z. A Solution Chemistry Approach to the Study of Rare Earth Element  
592 Precipitation by Oxalic Acid. *Metall and Materi Trans B* **1999**, *30* (2), 189–195.  
593 <https://doi.org/10.1007/s11663-999-0047-0>.
- 594(27) Khawassek, Y. M. Adsorption of Rare Earth Elements by Strong Acid Cation Exchange  
595 Resin Thermodynamics, Characteristics and Kinetics. 11.
- 596(28) Silva, R. G.; Morais, C. A.; Teixeira, L. V.; Oliveira, É. D. Selective Precipitation of  
597 High-Quality Rare Earth Oxalates or Carbonates from a Purified Sulfuric Liquor  
598 Containing Soluble Impurities. *Mining, Metallurgy & Exploration* **2019**, *36* (5), 967–  
599 977. <https://doi.org/10.1007/s42461-019-0090-6>.
- 600(29) Jorjani, E.; Shahbazi, M. The Production of Rare Earth Elements Group via Tributyl  
601 Phosphate Extraction and Precipitation Stripping Using Oxalic Acid. *Arabian Journal*  
602 *of Chemistry* **2016**, *9*, S1532–S1539. <https://doi.org/10.1016/j.arabjc.2012.04.002>.
- 603(30) Smith, R. M.; Martell, A. E. *Critical Stability Constants*; Springer US: Boston, MA,  
604 1989. <https://doi.org/10.1007/978-1-4615-6764-6>.
- 605(31) Martell, A. E.; Smith, R. M. *Other Organic Ligands*; Springer US: Boston, MA, 1977.  
606 <https://doi.org/10.1007/978-1-4757-1568-2>.
- 607(32) Ochsenkühn-Petropulu, M.; Lyberopulu, Th.; Ochsenkühn, K. M.; Parissakis, G.  
608 Recovery of Lanthanides and Yttrium from Red Mud by Selective Leaching. *Analytica*  
609 *Chimica Acta* **1996**, *319* (1–2), 249–254. [https://doi.org/10.1016/0003-2670\(95\)00486-](https://doi.org/10.1016/0003-2670(95)00486-6)  
610 [6](https://doi.org/10.1016/0003-2670(95)00486-6).

- 611(33) Liu, X.; Byrne, R. H. Rare Earth and Yttrium Phosphate Solubilities in Aqueous  
612 Solution. *Geochimica et Cosmochimica Acta* **1997**, 61 (8), 1625–1633.  
613 [https://doi.org/10.1016/S0016-7037\(97\)00037-9](https://doi.org/10.1016/S0016-7037(97)00037-9).
- 614(34) Li, X.-Z.; Zhou, L.-P.; Yan, L.-L.; Dong, Y.-M.; Bai, Z.-L.; Sun, X.-Q.; Diwu, J.; Wang,  
615 S.; Bünzli, J.-C.; Sun, Q.-F. A Supramolecular Lanthanide Separation Approach Based  
616 on Multivalent Cooperative Enhancement of Metal Ion Selectivity. *Nat Commun* **2018**,  
617 9 (1), 547. <https://doi.org/10.1038/s41467-018-02940-7>.
- 618(35) Deblonde, G. J.-P.; Mattocks, J. A.; Park, D. M.; Reed, D. W.; Cotruvo, J. A.; Jiao, Y.  
619 Selective and Efficient Biomacromolecular Extraction of Rare-Earth Elements Using  
620 Lanmodulin. *Inorg. Chem.* **2020**, 59 (17), 11855–11867.  
621 <https://doi.org/10.1021/acs.inorgchem.0c01303>.
- 622(36) Cotruvo, J. A.; Featherston, E. R.; Mattocks, J. A.; Ho, J. V.; Laremore, T. N.  
623 Lanmodulin: A Highly Selective Lanthanide-Binding Protein from a Lanthanide-  
624 Utilizing Bacterium. *J. Am. Chem. Soc.* **2018**, 140 (44), 15056–15061.  
625 <https://doi.org/10.1021/jacs.8b09842>.
- 626(37) Bau, M.; Tepe, N.; Mohwinkel, D. Siderophore-Promoted Transfer of Rare Earth  
627 Elements and Iron from Volcanic Ash into Glacial Meltwater, River and Ocean Water.  
628 *Earth and Planetary Science Letters* **2013**, 364, 30–36.  
629 <https://doi.org/10.1016/j.epsl.2013.01.002>.
- 630(38) Christenson, E. A.; Schijf, J. Stability of YREE Complexes with the Trihydroxamate  
631 Siderophore Desferrioxamine B at Seawater Ionic Strength. *Geochimica et*  
632 *Cosmochimica Acta* **2011**, 75 (22), 7047–7062.  
633 <https://doi.org/10.1016/j.gca.2011.09.022>.
- 634(39) Kraemer, D.; Kopf, S.; Bau, M. Oxidative Mobilization of Cerium and Uranium and  
635 Enhanced Release of “Immobile” High Field Strength Elements from Igneous Rocks in  
636 the Presence of the Biogenic Siderophore Desferrioxamine B. *Geochimica et*  
637 *Cosmochimica Acta* **2015**, 165, 263–279. <https://doi.org/10.1016/j.gca.2015.05.046>.
- 638(40) Canarini, A.; Kaiser, C.; Merchant, A.; Richter, A.; Wanek, W. Root Exudation of  
639 Primary Metabolites: Mechanisms and Their Roles in Plant Responses to  
640 Environmental Stimuli. *Front. Plant Sci.* **2019**, 10, 157.  
641 <https://doi.org/10.3389/fpls.2019.00157>.
- 642(41) Fathollahzadeh, H. Role of Microorganisms in Bioleaching of Rare Earth Elements  
643 from Primary and Secondary Resources. *Appl Microbiol Biotechnol* **2019**, 15.  
644(42) Mowafy, A. M. Biological Leaching of Rare Earth Elements. *World J Microbiol*  
645 *Biotechnol* **2020**, 36 (4), 61. <https://doi.org/10.1007/s11274-020-02838-x>.
- 646(43) Liu, C.; Sun, D.; Zheng, H.-X.; Wang, G.-B.; Liu, W.-S.; Cao, Y.; Tang, Y.-T.; Qiu, R.-  
647 L. The Limited Exclusion and Efficient Translocation Mediated by Organic Acids  
648 Contribute to Rare Earth Element Hyperaccumulation in *Phytolacca Americana*.  
649 *Science of The Total Environment* **2022**, 805, 150335.  
650 <https://doi.org/10.1016/j.scitotenv.2021.150335>.
- 651(44) Clarholm, M.; Skjellberg, U.; Rosling, A. Organic Acid Induced Release of Nutrients  
652 from Metal-Stabilized Soil Organic Matter – The Unbutton Model. *Soil Biology and*  
653 *Biochemistry* **2015**, 84, 168–176. <https://doi.org/10.1016/j.soilbio.2015.02.019>.
- 654(45) Mattocks, J. A.; Cotruvo, J. A. Biological, Biomolecular, and Bio-Inspired Strategies  
655 for Detection, Extraction, and Separations of Lanthanides and Actinides. *Chem. Soc.*  
656 *Rev.* **2020**, 49 (22), 8315–8334. <https://doi.org/10.1039/D0CS00653J>.
- 657(46) Osman, Y.; Gebreil, A.; Mowafy, A. M.; Anan, T. I.; Hamed, S. M. Characterization of  
658 *Aspergillus Niger* Siderophore That Mediates Bioleaching of Rare Earth Elements from  
659 Phosphorites. *World J Microbiol Biotechnol* **2019**, 35 (6), 93.  
660 <https://doi.org/10.1007/s11274-019-2666-1>.

661(47) Macías-Pérez, L. A.; Levard, C.; Barakat, M.; Angeletti, B.; Borschneck, D.; Poizat, L.;  
662 Achouak, W.; Auffan, M. Contrasted Microbial Community Colonization of a Bauxite  
663 Residue Deposit Marked by a Complex Geochemical Context. *Journal of Hazardous*  
664 *Materials* **2022**, 424, 127470. <https://doi.org/10.1016/j.jhazmat.2021.127470>.  
665(48) Fourier, C.; Luglia, M.; Hennebert, P.; Foulon, J.; Ambrosi, J.-P.; Angeletti, B.; Keller,  
666 C.; Criquet, S. Effects of Increasing Concentrations of Unamended and Gypsum  
667 Modified Bauxite Residues on Soil Microbial Community Functions and Structure – A  
668 Mesocosm Study. *Ecotoxicology and Environmental Safety* **2020**, 201, 110847.  
669 <https://doi.org/10.1016/j.ecoenv.2020.110847>.  
670(49) Fourier, C.; Luglia, M.; Keller, C.; Hennebert, P.; Foulon, J.; Ambrosi, J.-P.; Angeletti,  
671 B.; Criquet, S. How Raw and Gypsum Modified Bauxite Residues Affect Seed  
672 Germination, Enzyme Activities, and Root Development of *Sinapis Alba*. *Water Air*  
673 *Soil Pollut* **2021**, 232 (8), 309. <https://doi.org/10.1007/s11270-021-05232-x>.  
674  
675 **For Table of Contents Use Only**  
676

